Supplementary Material for Functional Network Dynamics of the Language System

Lucy R. Chai[1], Marcelo G. Mattar[1,2], Idan Asher Blank[3,4], Evelina Fedorenko[3,4,5], Danielle S. Bassett[1,6,7]

[1]*Department of Bioengineering, University of Pennsylvania, Philadelphia, PA 19104 USA*

[2]*Department of Psychology, University of Pennsylvania, Philadelphia, PA 19104 USA*

[3]*Department of Brain and Cognitive Sciences, Massachusetts Institute of Technology, Cambridge, MA 02139*

[4]*Department of Psychiatry, Harvard Medical School, Boston, MA, 02115 Harvard Medical School (Dept of Psychiatry), Boston, MA*

McGovern Institute for Brain Research, Massachusetts Institute of Technology, Cambridge, MA 02139

[5]*Department of Psychiatry, Massachusetts General Hospital, Charlestown, MA 02129 USA*

[6]*Department of Electrical & Systems Engineering, University of Pennsylvania, Philadelphia, PA 19104 USA*

[7]*Corresponding Author: dsb@seas.upenn.edu*

Supplementary Methods

1 Mathematics of community detection

We applied a community detection algorithm to obtain a partitioning of the nodes – or fROIs – of the language network into *communities* or *modules*. Nodes that are more strongly correlated in activity belong to the same module, while nodes that are less correlated in activity belong to different modules. Using a Louvain-like locally greedy algorithm (Blondel et al., 2008), we optimized a generalization of the modularity quality function (Newman, 2006; Porter et al., 2009) to the multilayer case (Mucha et al., 2010), which maximizes the quality of a partition of the fROIs into network communities that can vary over time windows (network layers). Networks with a high quality of partition can be sensibly divided into modules consisting of nodes with related activity patterns. The multilayer modularity is given by:

$$Q = \frac{1}{2\mu} \sum_{ijlr} \left\{ \left(A_{ijl} - \gamma_l V_{ijl} \right) \delta_{lr} + \delta_{ij} \omega_{jlr} \right\} \delta(g_{il}, g_{jr}) \tag{1}$$

where A_{ijl} is a pairwise correlation (or *edge*) between fROIs (or *nodes*) i and j in a time window l of the multilayer network, and V_{ijl} is the corresponding element of a specified null model. We use the Newman-Girvan null model within each layer: $V_{ijl} = \frac{k_{il} k_{jl}}{2m_l}$ where the total edge weight in layer l is $m_l = \frac{1}{2} \sum_{ij} A_{ijl}$ (i.e. the sum of all pairwise correlations in layer l), k_{il} refers to the intra-layer strength of node i in layer l (i.e. the sum of all pairwise correlations between node i and all other nodes in layer l), and k_{jl} is the intra-layer strength of node j in layer l. The parameter γ_l is a structural resolution parameter of layer l that can be used to tune the number of communities identified. The community assignment of node i in layer l is g_{il} , the community assignment of node

j in layer r is g_{jr}, and $\delta(g_{il}, g_{jr}) = 1$ if $g_{il} = g_{jr}$ and 0 otherwise. The correlation strength between node j in layer r and node j in layer l is ω_{jlr}. The total edge weight is $\mu = \frac{1}{2}\sum_{jr} \kappa_{jr}$, where $\kappa_{jl} = k_{jl} + c_{jl}$ is the strength of node j in layer l, k_{jl} is the intra-layer strength of node j in layer l, and $c_{jl} = \sum_r \omega_{jlr}$ is the inter-layer strength of node j in layer l. Because we are considering an ordinal case in which network layers are consecutive time windows, we let $\omega_{ijl} \equiv \omega = constant$ for neighboring layers, i.e. when $|l - r| = 1$. Otherwise, we let $\omega_{ijl} = 0$. Similarly, we set $\gamma = \gamma_l$ to a constant. We use $\omega = 0.5$ and $\gamma = 1$ in the analyses reported in the main text, and we test the robustness of our results to variations in these parameter choices in later sections of this Supplement. For each time window, a partition of the fROIs into communities was obtained by optimizing this multilayer modularity function, Q. Due to the stochastic nature of the algorithm and near degeneracy of the modularity landscape (Good et al., 2010), we performed this numerical optimization of the quality function 100 times for the network of language fROIs, separately for each participant and each run (Bassett et al., 2013a).

Supplementary Results

2 Robustness across parameters

The multislice community detection algorithm contains a structural resolution parameter γ and a temporal resolution parameter ω that must be selected prior to optimizing the multilayer modularity quality function (Mucha et al., 2010). The structural resolution parameter γ can be used to tune the size of communities identified: a small value of γ uncovers a few large communities, while a large value of γ uncovers many small communities. The temporal resolution parameter ω can be used to tune the temporal similarity of partitions: a small value of ω allows partitions to be quite different between network layers (time windows; e.g., see Bassett et al. (2011, 2013b, 2015)), while a large value of ω can be used to obtain a consistent partition across all network layers (e.g., see Cole et al. (2014)).

To find the optimal pair of structural and temporal resolution parameters, we ran a grid-search procedure that optimized the modularity function 100 times for each multilayer network, and for each pair of γ and ω values (Fig. 1A). Using this procedure, we identified combinations of parameters that fulfilled two criteria: (i) the pair of parameters yielded similar partitions across optimizations, suggesting consistency with the underlying network organization (Bassett et al., 2013a) (Fig. 1B), and (ii) the pair of parameters produced partitions in which nodes had neither an average flexibility of zero (i.e., node allegiances to communities remained static over time) nor an average flexibility of one (i.e., node allegiances to communities changed in every time window),

indicating sensitivity to dynamic reconfiguration but insensitivity to noise (Fig. 1C). Note that we calculated the similarity between partitions using the z-score of the Rand coefficient (Traud et al., 2011).

Searching the parameter space yielded $\gamma = 1$ and $\omega = 0.5$ as optimal values in which the partitions were consistent over optimizations, and yet the nodes were moderately flexible over time. Thus, these are the values that we used for the analyses reported in the main manuscript. However, it is important to note that the basic properties of the community structure of the network depended on the values chosen for the free parameters, as expected mathematically. We therefore tested whether the main results reported in the main manuscript were robust to small variations in the γ and ω values. We observed that the basic structure of the network remained reasonably constant in the range $\gamma \in [0.8, 1.2]$ and $\omega \in [0.4, 0.6]$. A similar two-module structure divided by left and right hemisphere exists in the module allegiance matrix for all pairs of γ and ω (Fig. 1D). Additionally, we observe correlated flexibilities when the flexibility of each node at each γ, ω pair is compared to the flexibility of each node when $\gamma = 1.0$ and $\omega = 0.5$ (Fig. 2). These findings indicate that the results described in the main manuscript are robust to small variations in structural and temporal resolution parameter values, supporting the reliability of the findings.

3 Robustness to window placement and reliability across scans

In the main text, we presented results obtained when dividing the fMRI data set of the semantic relatedness judgment task into 19 time windows, each lasting 20 TRs with a 50% overlap. We then

computed the measures of module allegiance and flexibility across all participants, runs, time windows, and optimizations. In this section, we present the results of the same analyses in two other ways. First, we present module allegiance and flexibility after using *non-overlapping* windows for the semantic relatedness judgement task, each 20 TRs in duration. Second, we use non-overlapping windows, each 10 TRs in duration (consistent with Cole et al. (2014)), that align with the stimuli presented during the semantic relatedness judgment task. In this second method, each time window contained data collected during either the number condition or the word condition, but not both.

Using non-overlapping windows that were 20 TRs in duration, we uncovered a consistent two-module structure in the module allegiance matrix. Additionally, we observed a high correlation between flexibility of language nodes with non-overlapping windows and the original nodes with overlapping windows ($r = 0.76$, $p < 0.001$, Fig. 3A).

Secondly, using non-overlapping windows that aligned with stimuli, we also obtained a similar network structure with a distinct separation into right and left modules for both number and word conditions, and correlated flexibility between nodes with non-overlapping, aligned time windows and nodes with the original overlapping time windows (number condition: $r = 0.65$, $p = 0.007$, word condition: $r = 0.66$, $p = 0.005$, Fig. 3B–C). These results suggest that the flexibility and module allegiance of the language network is robust to changes in window size and amount of overlap.

4 Robustness across tasks

In the main manuscript, we presented the results obtained when comparing the architecture of networks constructed from the semantic relatedness judgement task data to statistical null model networks. In this section, we present a similar analysis for the story comprehension task.

First, we compute the Rand z-score for partitions in different optimizations, and partitions in different time windows for each subject. We observe that the Rand z-score is significantly higher for partitions in different optimizations (two-sample t-test $t_{18} = 4.10$, $p < 0.001$, Hedges' g measure of effect size: $g = 1.76$, Fig. 4A), suggesting that partitions in different optimizations are more similar than partitions in different time windows. This indicates that variation across time is a bigger driver in the structure of the module allegiance matrix than variation across optimizations.

Next, we compare the actual data to static and nodal null models. We obtain qualitatively similar results in both tasks (Fig. 4). Using 100 static null model networks, we computed the null model module allegiance matrices for each subject and optimization for a single representative null model. We then computed the equivalent module allegiance matrices in the real data, again for each subject, optimization, and run, and compute the equivalent module allegiance matrices in the real data. We observed significant differences in the two distributions (two-sample ks-test $k = 0.343$, $p = 0$, Fig. 4B). Next, we compute module allegiance matrices for the nodal null networks from the second story. We computed the module allegiance matrix for each subject, averaged over all optimizations and null models, and measured the average module allegiance in the left hemisphere, right hemisphere, and between hemispheres. We then computed the corresponding values in the

real data. We observed significant differences between the real data and the null models in the left and right hemispheres (paired t-test left: $t_9 = 5.80$, $p < 0.001$ Hedges' $g = 2.54$, right: $t_9 = 6.73$, $p < 0.001$, $g = 2.42$). The difference between hemispheres was not significantly different from the random null models (paired t-test $t_9 = -0.97$, $p = 0.356$, $g = -0.354$, Fig. 4C). These results indicate that the two modules – while distinct and sensitive to the different anatomical roles of each hemisphere – nevertheless display nontrivial dynamic functional interactions. Lastly, we observe that the distribution of data across all static null models (Fig. 4D) is qualitatively similar to the distribution of a single null model. However, we focused on one null model when comparing the null model to real data to maintain the same number of data points across both distributions.

5 Robustness across different stories

In the main text, we presented results for module allegiance, laterality, and flexibility during the comprehension of a single story. Here, we present results for the remainder of the stories presented to subjects during fMRI data acquisition. In total there were 8 different stories presented to subjects, and between 1 and 10 subjects listened to each story. Across all stories, we observed a consistent two module structure in the module allegiance matrix (see Fig. 5). In Table 1, we provide the results of statistical tests demonstrating that module allegiance values were lower between hemispheres than within hemispheres.

6 Network Effects of Low Connectivity Strengths

To determine the effects of regions with low functional connectivity on the resulting network structure, we thresholded the functional connectivity matrices to remove correlations below 0.10, 0.25, 0.50, and 0.90 in absolute value. We then computed module allegiance and flexibility as was done with the unthresholded functional connectivity matrices. We observed a similar separation by hemisphere in the module allegiance matrices, and highly correlated flexibility values up to the 0.50 threshold. These results suggest that the network structure is driven by changes in high functional connectivity strengths rather than low functional connectivity strengths.

7 Activation Maps

Activation maps of the subjects during the language localizer task (sentences>nonwords contrast) and the semantic relatedness judgment task (semantic $>$ number contrast) show robust activations corresponding to the 16 defined language fROIs. The activation maps are thresholded with a p-value of $p < 0.001$. Only the positive intensities are displayed.

Supplementary Discussion

8 Dynamic reconfiguration of brain networks.

Advances in dynamic network-based techniques from applied mathematics have opened exciting new avenues for characterizing neural architectures across many species from humans to rodents

(Hutchison et al., 2013; Keilholz et al., 2013). Here, we use these approaches to study the dynamic functional interactions that accompany and enable language processing in humans. Using a static network null model, we first demonstrate that language – like other cognitive functions such as learning (Bassett et al., 2011, 2013b, 2015; Mantzaris et al., 2013) and memory (Braun et al., 2015; Siebenhuhner et al., 2013) – displays temporally varying functional connectivity patterns (Mattar et al., 2015). This network reconfiguration is differentially driven by different brain areas, with some highly variable regions and other regions that are more stable in their functional interactions. Our results highlight the dimension of time, which is rarely addressed in fMRI studies. By using tools from dynamic network analysis, we are able to portray the changing states of the brain during language processing and apply novel metrics that take into account the temporal variability of functional network architecture.

9 Methological Considerations

There are a few methological considerations pertinent to this work. First, we collected fMRI data from a total of 22 subjects, ten participants for the story task and twelve participants for the semantic relatedness judgment task. Second, subjects performed two language tasks that were fundamentally different in nature. Yet, using these distinct tasks enabled us to investigate consistencies within the language network architecture across the two tasks. We observed similar lateralized patterns in both tasks, suggesting that the modular organization of the language network is robust and not dependent on the type of language task being performed. Third, alternate methods also exist for the characterization of the non-stationarity of fROIs, such as fitting a vector autoregressive

(VAR) model as a measure of dynamics (Chang and Glover, 2010). Here, we applied a complementary approach based on a temporal null model–random shufflings of network layers (Bassett et al., 2013b).

A fourth important consideration lies in the choice of localizer task. Since our earlier work in 2010 (Fedorenko et al., 2010), we have re-generated the functional language parcels using large sets of subjects run on a passive-reading version of the localizer. The regions that emerge from this localizer are similar to those studied here (Fedorenko, 2014). Furthermore, we observe that the activations in the high-level language processing regions studied here are extremely robust to task and many other features of the localizer, including the materials, modality of presentation, and language for full bilinguals (Fedorenko, 2014). Thus, due to the similarities between parcels defined using the passive reading localizer and the memory probe, the presence of the memory probe tasks in some of the subjects' data used for generating the functional language parcels and its absence in the participants tested here is unlikely to capture the different cognitive strategies involved in the memory component of the localizer.

References

Bassett DS, Porter MA, Wymbs NF, Grafton ST, Carlson JM, Mucha PJ. 2013a. Robust detection of dynamic community structure in networks. Chaos: An Interdisciplinary Journal of Nonlinear Science. 23:013142.

Bassett DS, Wymbs NF, Porter MA, Mucha PJ, Carlson JM, Grafton ST. 2011. Dynamic reconfiguration of human brain networks during learning. Proc Natl Acad Sci U S A. 108:7641–7646.

Bassett DS, Wymbs NF, Rombach MP, Porter MA, Mucha PJ, Grafton ST. 2013b. Task-based core-periphery organization of human brain dynamics. PLoS Comput Biol. 9:e1003171.

Bassett DS, Yang M, Wymbs NF, Grafton ST. 2015. Learning-induced autonomy of sensorimotor systems. Nature Neurosci. 18:744–751.

Blondel VD, Guillaume JL, Lambiotte R, Lefebvre E. 2008. Fast unfolding of communities in large networks. Journal of Statistical Mechanics: Theory and Experiment. 2008:P10008.

Braun U, Schafer A, Walter H, Erk S, Romanczuk-Seiferth N, Haddad L, Schweiger JI, Grimm O, Heinz A, Tost H, Meyer-Lindenberg A, Bassett DS. 2015. Dynamic reconfiguration of frontal brain networks during executive cognition in humans. Proc Natl Acad Sci U S A. 112:11678–11683.

Chang C, Glover GH. 2010. Time–frequency dynamics of resting-state brain connectivity measured with fmri. Neuroimage. 50:81–98.

Cole MW, Bassett DS, Power JD, Braver TS, Petersen SE. 2014. Intrinsic and task-evoked network architectures of the human brain. Neuron. 83:238–251.

Fedorenko E. 2014. The role of domain-general cognitive control in language comprehension. Frontiers in psychology. 5.

Fedorenko E, Hsieh PJ, Nieto-Castanon A, Whitfield-Gabrieli S, Kanwisher N. 2010. New method for fMRI investigations of language: defining ROIs functionally in individual subjects. J Neurophysiol. 104:1177–1194.

Good BH, de Montjoye YA, Clauset A. 2010. Performance of modularity maximization in practical contexts. Phys Rev E. 81:046106.

Hutchison RM, Womelsdorf T, Allen EA, Bandettini PA, Calhoun VD, Corbetta M, Della Penna S, Duyn JH, Glover GH, Gonzalez-Castillo J, Handwerker DA, Keilholz S, Kiviniemi V, Leopold DA, de Pasquale F, Sporns O, Walter M, Chang C. 2013. Dynamic functional connectivity: promise, issues, and interpretations. Neuroimage. 80:360–378.

Keilholz SD, Magnuson ME, Pan WJ, Willis M, Thompson GJ. 2013. Dynamic properties of functional connectivity in the rodent. Brain Connect. 3:31–40.

Mantzaris AV, Bassett DS, Wymbs NF, Estrada E, Porter MA, Mucha PJ, Grafton ST, Higham DJ. 2013. Dynamic network centrality summarizes learning in the human brain. Journal of Complex Networks. 1:83–92.

Mattar M, Cole MW, Thompson-Schill SL, Bassett DS. 2015. A functional cartography of cognitive systems. PLoS Comp Biol. Provisionally Accepted.

Mucha PJ, Richardson T, Macon K, Porter MA, Onnela JP. 2010. Community sturucture in time-dependent, multiscle, and multiplex networks. Science. 328:876–878.

Newman ME. 2006. Modularity and community structure in networks. Proc Natl Acad Sci U S A. 103:8577–8582.

Porter MA, Onnela JP, Mucha PJ. 2009. Communities in networks. Notices of the AMS. 56:1082–1097.

Siebenhuhner F, Wiess SA, Coppola R, Weinberger DR, Bassett DS. 2013. Intra- and inter-frequency brain network structure in health and schizophrenia. PLoS One. 8:e72351.

Traud AL, Kelsic ED, Mucha P, Porter MA. 2011. Comparing community structure to characteristics in online collegiate social networks. SIAM Review. 53:526–542.

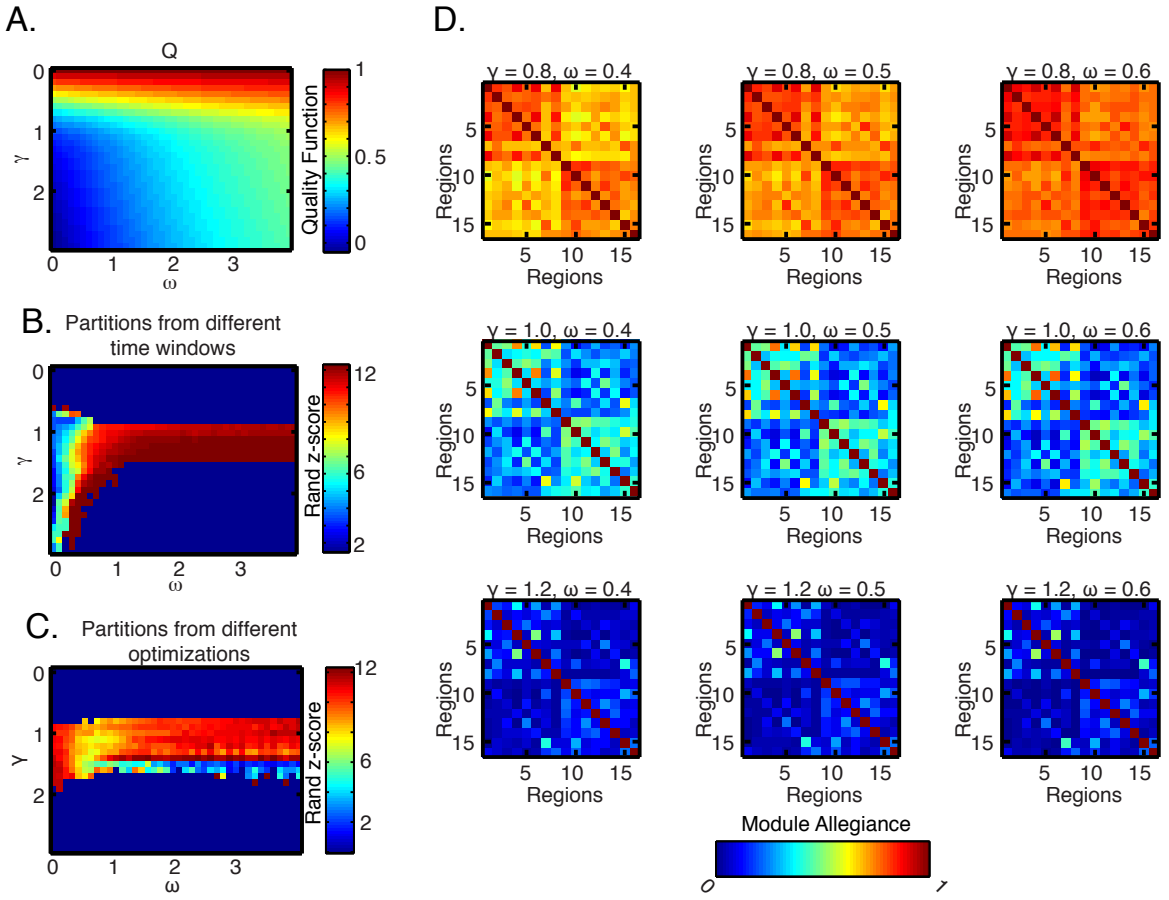

Figure 1: **Effect of structural and temporal resolution parameters.** *(A)* The average value of the modularity quality index, Q, obtained by optimizing a multilayer modularity quality function using a Louvain-like locally greedy algorithm *(left)*. *(B)* We searched for (γ, ω) pairs that yielded partitions that were relatively variable over time, resulting in a moderate z-score of the Rand coefficient over network layers (or time windows) *(middle)*. *(C)* Additionally, we searched for parameter pairs that yielded consistent partitions in each optimization of the multilayer quality function, resulting in a high z-score of the Rand coefficient over partitions *(right)*. When selecting the parameter pair for the results reported in the main manuscript, we considered both consistency of partitions over optimizations and moderate flexibility of partitions over time. *(D)* Module allegiance matricies computed from various values of γ and ω parameters revealed a consistent two-module structure.

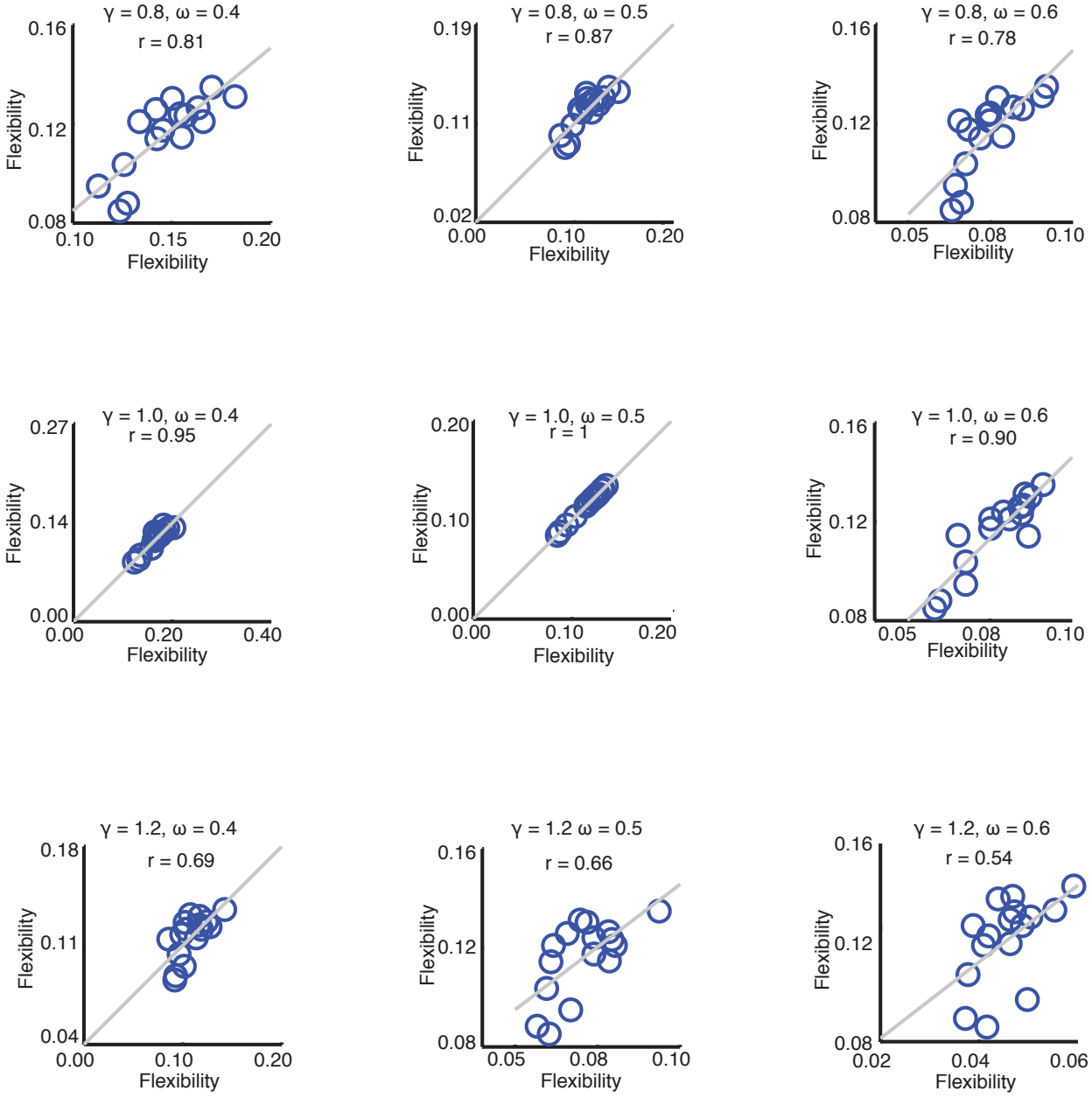

Figure 2: **Robustness of flexibility across structural and temporal resolution parameters.** Correlation between (i) node flexibility obtained using various values of the γ and ω parameters and (ii) node flexibility obtained using $\gamma = 1.0$ and $\omega = 0.5$ (the values used for the results reported in the main manuscript).

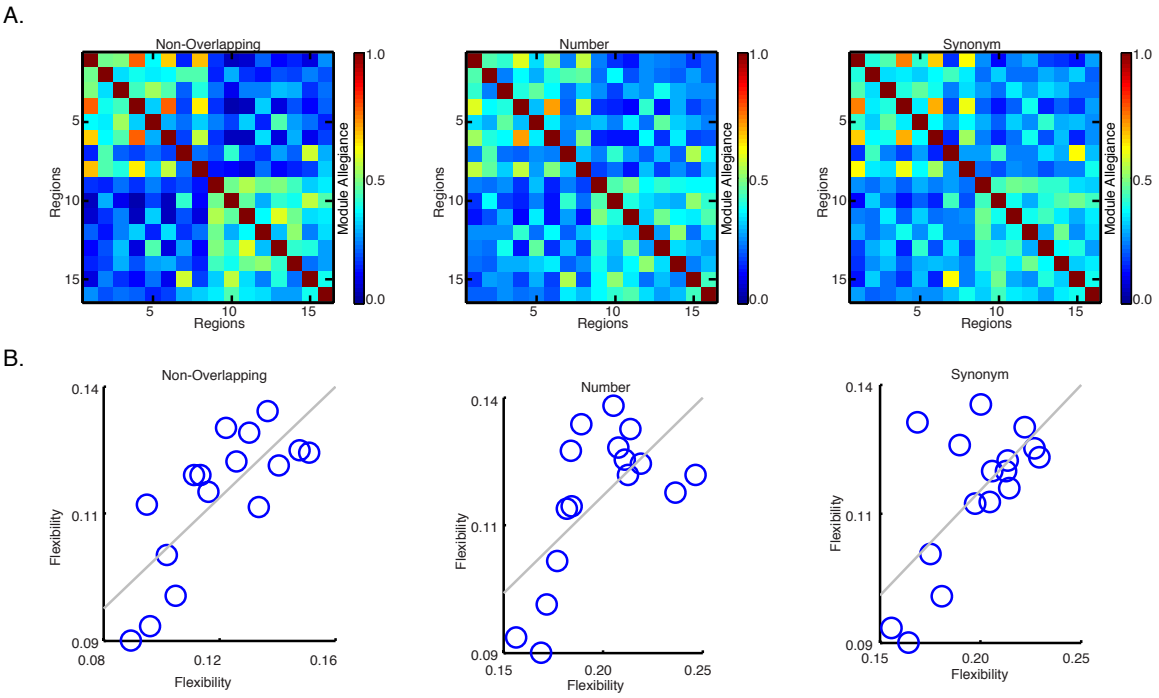

Figure 3: **Effect of changing time window overlap and duration.** *(A)* Module allegiance matrix computed from non-overlapping windows 20 TRs in length *(top)*. Correlation between flexibility of nodes with non-overlapping windows, and flexibility of nodes with 20 TR overlapping windows *(bottom)*. *(B)* Module allegiance matrix computed from non-overlapping windows 10 TRs in length, capturing only the number condition of the semantic relatedness judgment task *(top)*. Correlation between flexibility of nodes with non-overlapping windows of only the number condition, and flexibility of nodes with 20 TR overlapping windows *(bottom)*. *(C)* Module allegiance matrix obtained from using 10 TR non-overlapping windows, capturing only the word condition of the semantic relatedness judgment task *(top)*. Correlation between flexibility of nodes with non-overlapping windows of the word condition, and flexibility of nodes with 20 TR overlapping windows *(bottom)*.

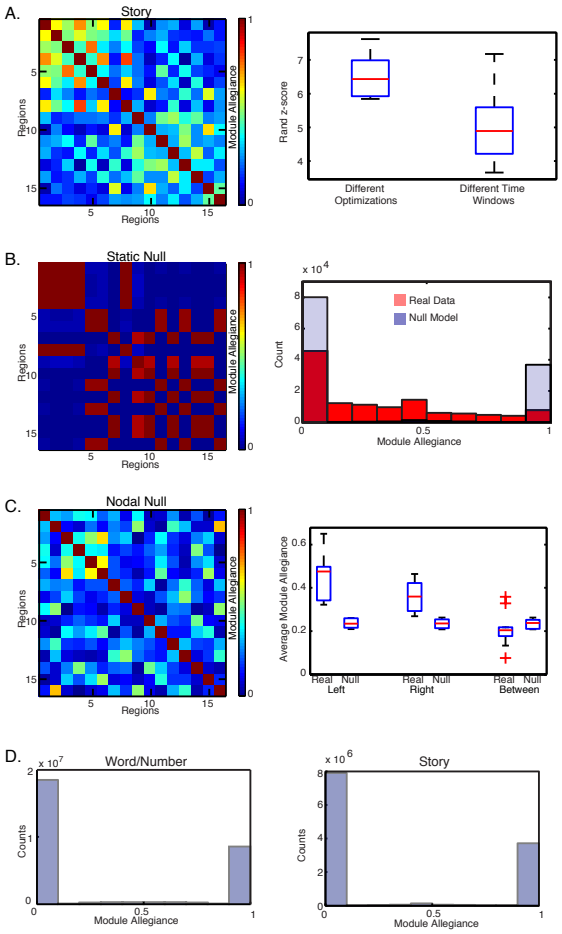

Figure 4: **Comparison of story comprehension task to null models.** *(A)* Module allegiance matrix obtained from the second story of the story comprehension data *(left)*. We observe more similarity in partitions from different optimizations than partitions from different time windows *(right)*. *(B)* Module allegiance matrix of a representative static null model, obtained from a single multilayer association matrix *(left)*. Histogram of the distribution of module allegiance values computed for each subject and optimization, compared to the distribution of module allegiance values of a representative null model, for each subject and optimization *(right)*. *(C)* Module allegiance matrix of a representative nodal null model, obtained from a single multilayer association matrix *(left)*. Boxplot showing the difference in the average value of module allegiance for each subject in the left hemisphere, right hemisphere, and between hemispheres for real and nodal null model module allegiance matrices *(right)*. *(D)* Distribution of module allegiance values for the semantic relatedness task *(left)* and the story comprehension task *(right)* over all 100 static null models.

Table 1: Story Comprehension Task

	Number of Subjects:	MA LH-Btw:	MA RH-Btw	MA LH-RH
Story 1	9	$t_{16} = 4.54$, $p < 0.001$	$t_{16} = 5.69$, $p < 0.001$	$t_{16} = 1.36$, $p = 0.19$
Story 2	10	$t_{18} = 5.44$, $p < 0.001$	$t_{18} = 4.41$, $p < 0.001$	$t_{18} = 2.31$, $p = 0.03$
Story 3	9	$t_{16} = 4.73$, $p < 0.001$	$t_{16} = 3.22$, $p = 0.005$	$t_{16} = 1.94$, $p = 0.07$
Story 4	10	$t_{18} = 5.60$, $p < 0.001$	$t_{18} = 5.76$, $p < 0.001$	$t_{18} = 1.47$, $p = 0.16$
Story 5	9	$t_{16} = 5.35$, $p < 0.001$	$t_{16} = 3.68$, $p = 0.005$	$t_{16} = 2.91$, $p = 0.01$
Story 6	2	$t_{2} = 1.04$, $p = 0.41$	$t_{2} = 1.04$, $p = 0.41$	$t_{2} = 0.47$, $p = 0.68$
Story 7	3	$t_{4} = 5.75$, $p = 0.004$	$t_{4} = 3.02$, $p = 0.03$	$t_{4} = 2.14$, $p = 0.09$
Story 9	1			

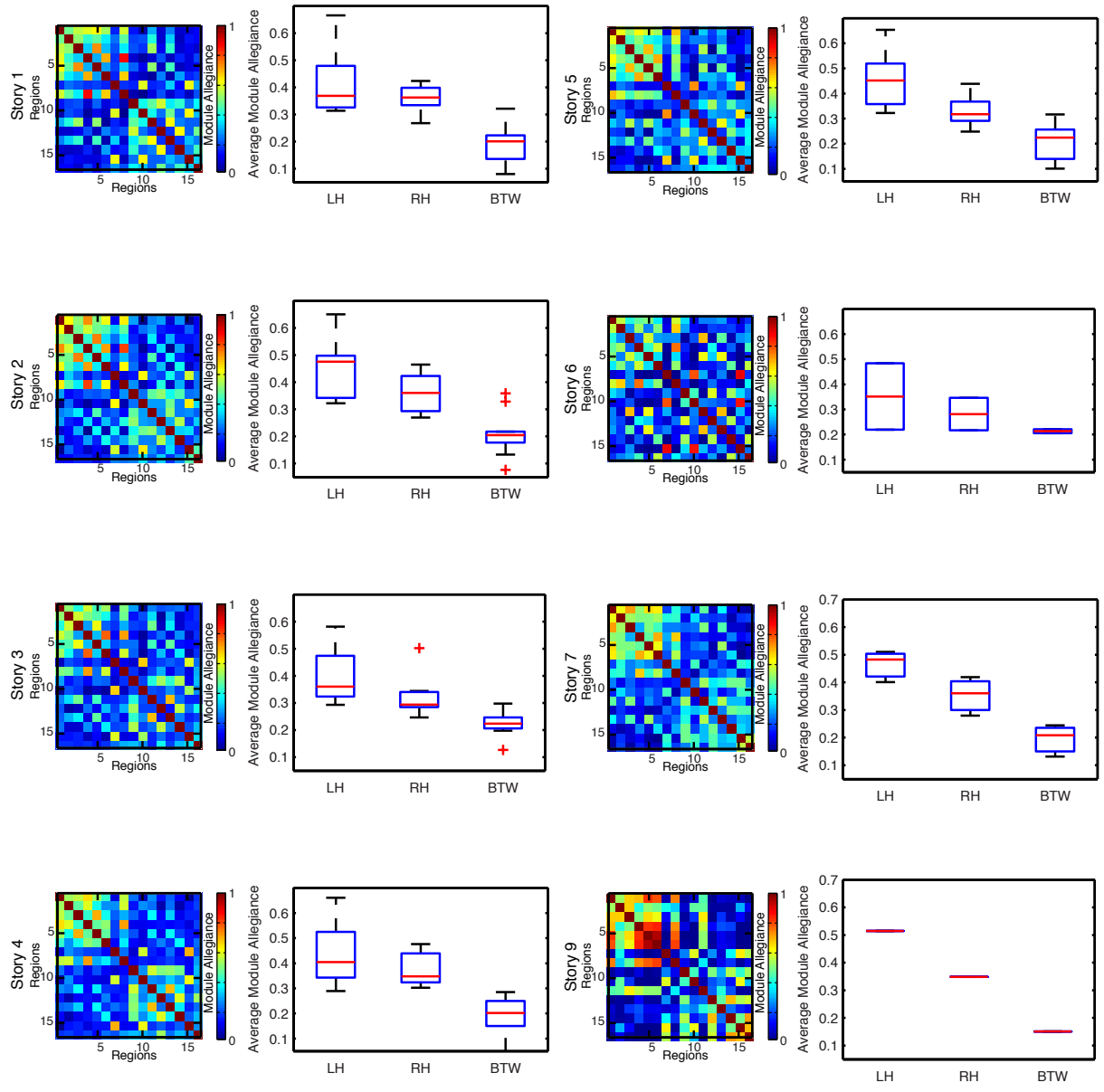

Figure 5: **Module allegiance of story comprehension tasks.** In the module allegiance matrices for each story, we observe a consistent two-module architecture separated by left and right hemisphere. Furthermore, we observe that the average module allegiance within hemispheres is greater than the average module allegiance between hemispheres. Boxplots illustrate the average module allegiance within the left hemisphere, within the right hemisphere, and between hemispheres for each story, where whiskers illustrate variation between subjects.

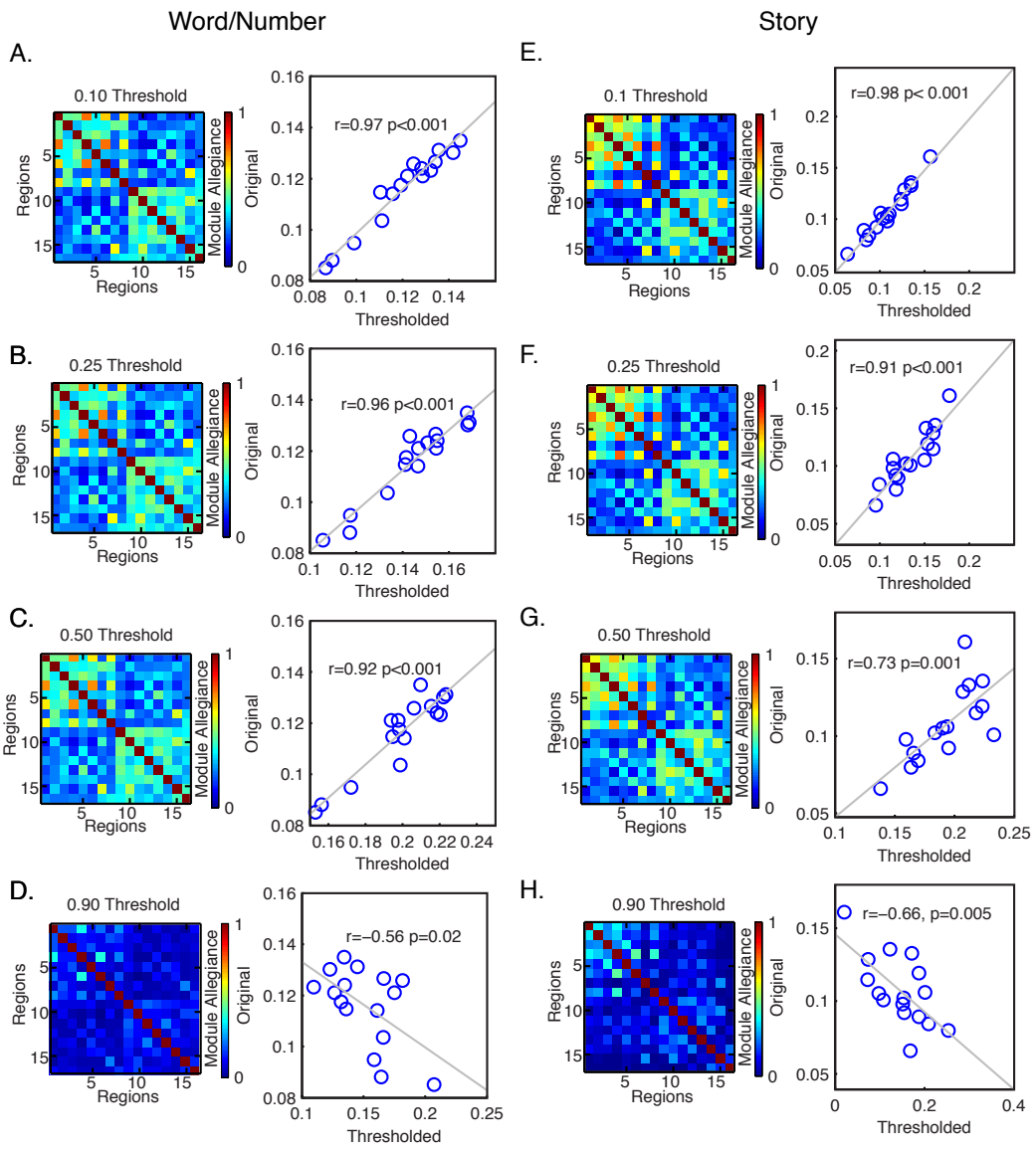

Figure 6: **Effect of Removing Low Correlations.** For the semantic relatedness judgment task, we thresholded functional connectivity matrices to remove correlations below 0.10 *(A)*, below 0.25 *(B)*, below 0.50 *(C)*, and below 0.90 *(D)* in absolute value. We computed module allegiance from the thresholded functional connectivity *(left)*, and the correlation between the flexibility using the thresholded functional connectivity versus unthresholded functional connectivity *(right)*. Similarly for the story comprehension task, we thresholded functional connectivity matrices to remove correlations below 0.10 *(A)*, below 0.25 *(B)*, below 0.50 *(C)*, and below 0.90 *(D)* in absolute value. We computed module allegiance from the thresholded functional connectivity *(left)*, and the correlation between the flexibility using the thresholded functional connectivity versus unthresholded functional connectivity *(right)*.

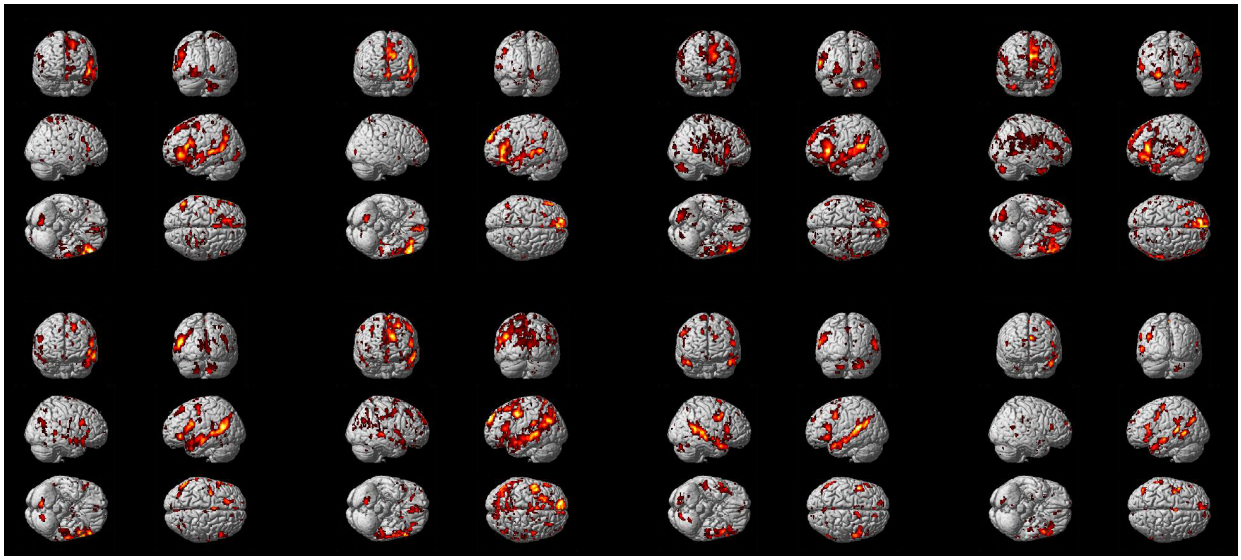

Figure 7: **Activation maps during task and localizer.** Activation maps for four of twelve subjects during the semantic relatedness judgment task (top), and the language localizer (bottom).

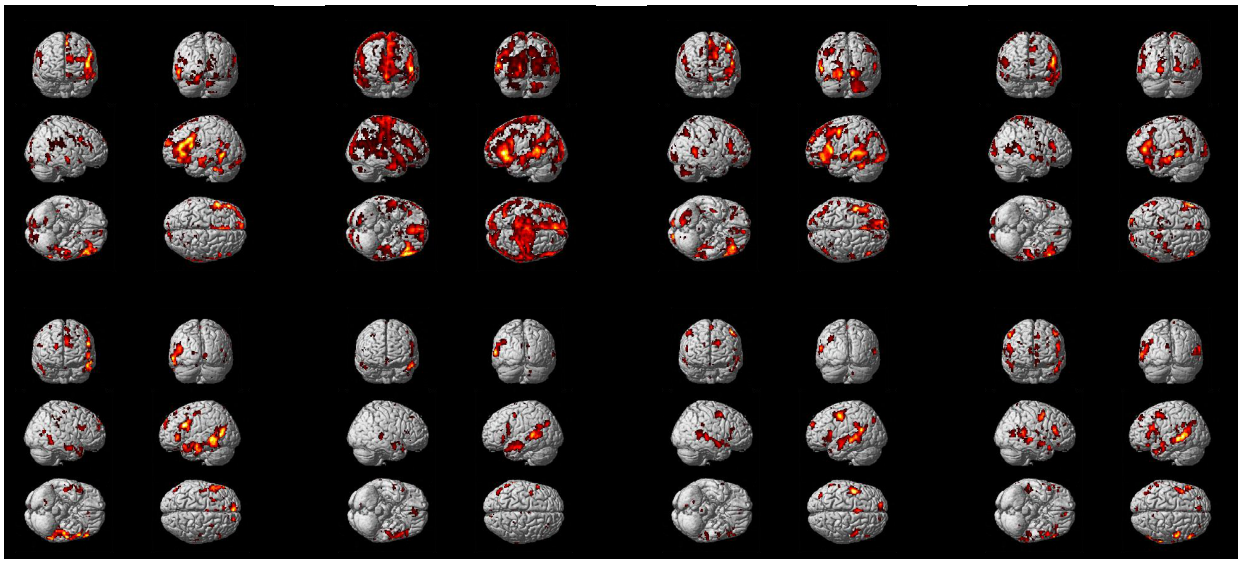

Figure 8: **Activation maps during task and localizer.** Activation maps for four of twelve subjects during the semantic relatedness judgment task (top), and the language localizer (bottom).

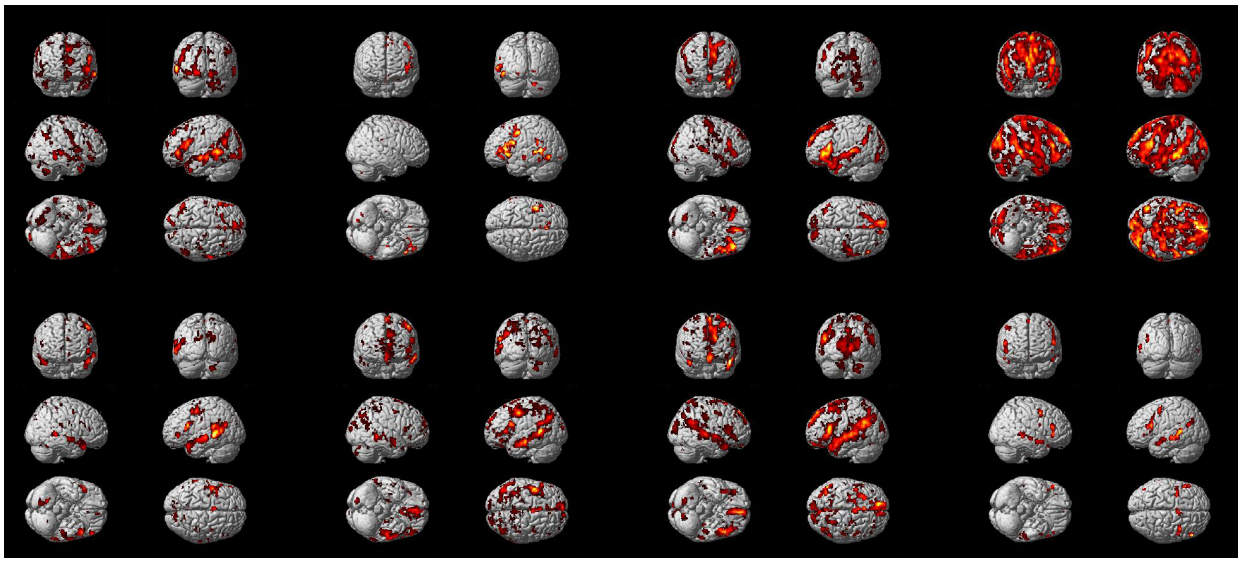

Figure 9: **Activation maps during task and localizer.** Activation maps for four of twelve subjects during the semantic relatedness judgment task (top), and the language localizer (bottom).